Oxidative stress-mediated protein conformation changes: ESR study of spin-labelled staphylococcal nuclease

2007 J. Phys.: Condens. Matter 19 285201

(http://iopscience.iop.org/0953-8984/19/28/285201)

IOP PUBLISHING JOURNAL OF PHYSICS: CONDENSED MATTER

J. Phys.: Condens. Matter **19** (2007) 285201 (13pp) doi:10.1088/0953-8984/19/28/285201

Oxidative stress-mediated protein conformation changes: ESR study of spin-labelled staphylococcal nuclease

Andrzej Sienkiewicz[1,2,5], Bertrand Vileno[1], Katarzyna Pierzchała[1,2], Mariusz Czuba[3], Pierre Marcoux[1], Alfreda Graczyk[3], Piotr G Fajer[4] and László Forró[1]

[1] Institute of Physics of Complex Matter, Ecole Polytechnique Fédérale, CH-1015 Lausanne, Switzerland
[2] Institute of Physics, Polish Academy of Sciences, Aleja Lotników 32/46, 02-668 Warsaw, Poland
[3] Institute of Optoelectronics, Military University of Technology, ulica Kaliskiego 2, 00-908 Warsaw, Poland
[4] National High Magnetic Field Laboratory, Florida State University, Tallahassee, FL 32310, USA

E-mail: Andrzej.Sienkiewicz@epfl.ch

Received 6 November 2006
Published 25 June 2007
Online at stacks.iop.org/JPhysCM/19/285201

Abstract

We report on the electron spin resonance (ESR) study of the photo-oxidative stress-mediated protein conformation changes in the spin-labelled protein staphylococcal nuclease (SNase). The photo-oxidative stress was brought on by photosensitization of singlet oxygen ($^1\Delta_g$) in the presence of a novel photosensitizer, water-soluble fullerol $C_{60}(OH)_{19}(ONa)_{17}$, and resulted in partial protein denaturation. This process was monitored via ESR measurements performed for a spin-labelled SNase Thr-62-Cys mutant, with MTSSL spin label (SL) attached to the cysteine 62 residue (SNase T62C-SL). Prior to ESR measurements of the oxidative stress-induced alterations in protein conformations, the efficiency of $C_{60}(OH)_{19}(ONa)_{17}$ for $^1\Delta_g$-generation was confirmed by three different techniques: (i) selective reactive scavenging of $^1\Delta_g$ and ESR detection of the resulting paramagnetic product, (ii) $^1\Delta_g$-mediated photo-oxidative loss of tryptophan and (iii) by measuring the characteristic near-infrared phosphorescence of singlet oxygen at 1270 nm. The observed evolution of the ESR spectra of SNase T62C-SL as a function of exposure to the photo-oxidative stress points to marked changes in protein conformation due to the deleterious action of $^1\Delta_g$.

[5] Author to whom any correspondence should be addressed.

1. Introduction

Significant evidence points to oxidative stress (OS)-mediated damage as a major factor in the initiation and progression of numerous age-related diseases, including skin cancers, age-related macular degeneration, Alzheimer's and Parkinson's diseases and age-related cataract [1, 2]. It is thought that the oxidative damage to cells is directly related to the levels of reactive oxygen species (ROS), like, for example, superoxide radical ($O_2^{-\bullet}$), hydrogen peroxide (H_2O_2) or hydroxyl radical ($^\bullet$OH). In normal living cells generation of ROS belongs to a common mechanism that underlies different forms of cellular functions. In excess, however, generation of ROS may lead to pathophysiological processes, such as necrosis, apoptosis and excitotoxicity in normal ageing, ischaemia and neurodegenerative diseases [3]. In living cells, OS occurs when the level of pro-oxidants, i.e. ROS, exceeds the ability of the cell to respond through antioxidant defence. This ultimately leads to modification and degradation of cellular proteins, damage to phospholipids, DNA and mitochondria, and might result in cell death [4]. Proteins comprise about 70% of the dry weight of cells and because of their abundance are major targets for OS-induced damage [5]. A number of studies associate OS-mediated changes in protein conformation with various cellular dysfunctions observed during ageing and age-related neurodegenerative diseases [6].

The lowest excited electronic state of molecular oxygen, singlet oxygen ($^1\Delta_g$), constitutes a part of the intracellular milieu of ROS that arise from cellular processes or exogenous chemical agents. Generated in biological systems, $^1\Delta_g$ can serve as a signalling molecule as well as an initiator of detrimental biological oxidations [7]. Ever since a relation between ROS, such as $^\bullet$OH, $O_2^{-\bullet}$, H_2O_2 and $^1\Delta_g$, and various diseases was suggested, much effort has been made to follow the generation pathways of ROS and the fate of their biomolecular targets. In particular, it has been shown that light-induced singlet oxygen is a key player in photo-inactivation of proteins in human skin, ultimately resulting in skin ageing and formation of skin cancer [8]. Since proteins dominate the quenching of singlet oxygen in cell membranes and cytosol, considerable efforts have been made to comprehend $^1\Delta_g$-mediated damage to proteins. It is thought that $^1\Delta_g$-induced alterations in proteins proceed, in most cases, via the degradation of the five photo-oxidizable amino acids, i.e. tryptophan, histidine, tyrosine, methionine and cysteine [9]. Reactions of $^1\Delta_g$ with each of these residues give rise to further reactive species. The photosensitized oxidation of proteins has been extensively reviewed and the investigations have been focused on kinetics and the identification of reaction products [10]. Much less is known, however, about singlet oxygen-mediated conformation changes of the protein structures and their biological consequences [5].

Very often, in living systems and laboratory conditions, generation of ROS and $^1\Delta_g$ occurs under illumination with light and in the presence of photoactive molecules, called photosensitizers (PS). Depending on their photophysical properties and surrounding conditions, PS can generate different varieties of ROS that may have either detrimental or beneficial impact on their immediate environment [11]. In particular, since PS-mediated production of ROS on a large scale generates damages to cells, PS that accumulate in tissues have been implemented in photodynamic cancer therapy (PDT) [12]. Photo-generation of ROS in the presence of PS has traditionally been defined as occurring via two major routes. The first of these includes direct involvement of the light-excited PS in the photo-oxidation processes through electron or hydrogen transfer/exchange, which results in the generation of free radicals. These mechanisms are often referred to as type I processes. The second major process involves indirect oxidation of the biological targets via the formation and subsequent reactions of singlet oxygen, which is generated by energy transfer from the light-excited PS in its triplet state to the ground state of

molecular oxygen, which is also triplet ($^3\Sigma_g^-$). This mechanism is often referred to as type II process.

Fullerenes are carbon nanoparticles that have a characteristic cage structure and offer unique promise for use in newly developing electronic as well as in optical and biomedical materials and applications. Due to their unique photochemical and photophysical properties, fullerene C_{60}-based derivatives have attracted a lot of attention as potent PS for the light-induced production of ROS. It has been shown that water-soluble derivatives of C_{60}, with various functional groups (e.g. –OH, –COOH, $–NH_2$) attached to the fullerene cage, are promising candidates for biomedical applications [13]. Poly-hydroxylated fullerenes, fullerols, seem to be particularly intriguing, since depending on the method of their use, they might behave either as efficient antioxidants, thus reducing ROS levels in cells and tissues [14], or be producers of ROS under illumination with visible or UV light [15–17]. It is also generally thought that hydroxylation of the fullerene cage reduces the net generation of singlet oxygen [18, 19]. A recent differential toxicity study of some water-soluble fullerene species demonstrated that changes in the fullerene cage structure directly affected the cytotoxicity *in vitro*. In particular, water-soluble nano-C_{60} demonstrated significant cytotoxicity to tissue culture cells, but a highly hydroxylated water-soluble fullerene, $C_{60}(OH)_{24}$, produced no evidence of cytotoxicity under the same conditions [20].

In our previous study we have shown that a commercially available fullerol, C_{60} $(OH)_{24}$, was a good PS for the formation of singlet oxygen in aqueous milieus [16]. Herein we report on the photophysical properties of the custom-made water-soluble fullerol $C_{60}(OH)_{19}(ONa)_{17}$. In contrast to the fullerol $C_{60}(OH)_{24}$, the newly synthesized compound has a substantially larger degree of functionalization (36 oxidized carbons per C_{60} cage) and reveals even better water solubility (up to 8 mg ml^{-1}). Since it is generally accepted that increasing functionalization of the fullerene cage impairs the formation of singlet oxygen via a type II process, thus shifting its major route of action to type I mechanisms, we implemented several spectroscopic tools to characterize this novel photosensitizing compound. In particular, the photo-efficiency of fullerol $C_{60}(OH)_{19}(ONa)_{17}$ for the generation of singlet oxygen was studied by three different techniques: (i) selective reactive scavenging of $^1\Delta_g$, which was followed by ESR detection of the resulting paramagnetic product, (ii) by measuring the characteristic near-infrared phosphorescence of $^1\Delta_g$ at 1270 nm, and (iii) by $^1\Delta_g$-mediated photo-oxidative loss of tryptophan. We also used fullerol $C_{60}(OH)_{19}(ONa)_{17}$ as a photosensitizer in the study of OS-mediated conformation changes in staphylococcal nuclease (SNase), a toxic protein from the bacterium *Staphylococcus aureus*. Since we implemented an ESR technique to achieve this goal, the actual protein used in this work was a spin-labelled Thr-62-Cys SNase mutant, with MTSSL spin label (SL) attached to the cysteine 62 residue (SNase T62C-SL).

All evidence indicates that fullerol $C_{60}(OH)_{19}(ONa)_{17}$ generates singlet oxygen in aqueous solutions. Moreover, marked alterations in the ESR spectra acquired for the spin-labelled SNase mutant (SNase T62C-SL), which was exposed to the photo-oxidative stress in the presence of fullerol $C_{60}(OH)_{19}(ONa)_{17}$, suggested that the oxidative stress induced changes in the protein conformation. Thus, in the present study, we demonstrate that the highly hydroxylated fullerene derivative may not necessarily behave as a 'free radical sponge', as has been suggested in many recent reports [19–21]. In contrast, under certain conditions, it can also generate the strongly oxidative agent, singlet oxygen.

2. Materials and methods

2.1. Photosensitizer

The highly derivatized fullerol $C_{60}(OH)_{19}(ONa)_{17}$, with 36 oxidized carbons per C_{60} cage, was synthesized under acidic conditions using the approach suggested by Chiang *et al* [22] and

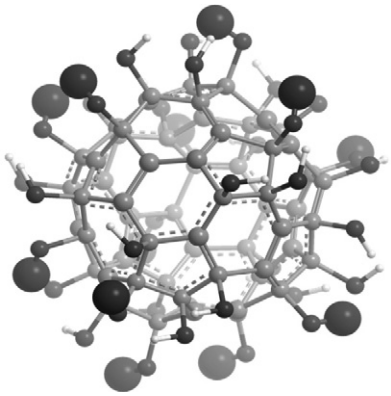

Figure 1. A ball-and-stick representation of the atomic structure of the custom-made fullerol $C_{60}(OH)_{19}(ONa)_{17}$. Carbon atoms are depicted by small-size light-grey spheres. Oxygen atoms are depicted by small-size dark spheres. The first-plan sodium atoms are depicted by large dark spheres. The further-plan sodium atoms are shown as large grey spheres. Hydrogen atoms are shown as small white spheres.

described in detail by Vileno *et al* [17]. The final product, in the form of a brown powder, has a very high solubility in water, reaching 8 mg ml^{-1}. A schematic representation of the molecular structure of the custom-made fullerol $C_{60}(OH)_{19}(ONa)_{17}$ is shown in figure 1.

2.2. ESR detection of singlet oxygen

The photosensitized generation of singlet oxygen in the presence of fullerol $C_{60}(OH)_{19}(ONa)_{17}$ was detected in the aqueous milieus of D_2O and H_2O by EPR using a singlet oxygen-scavenging reagent, 2,2,6,6-tetramethyl-4-piperidinol (TMP–OH) from Sigma. The diamagnetic TMP–OH reacts with singlet oxygen, thus yielding a paramagnetic product, TEMPOL. This approach, first introduced by Lion *et al* [23], is thought to be highly specific to the formation of singlet oxygen [24]. The stock solutions containing 25 mM TMP–OH and 0.25 mM of fullerol $C_{60}(OH)_{19}(ONa)_{17}$ were saturated with oxygen (by bubbling O_2 for 20 min). For performing ESR measurements, aliquots of about 7 ml were transferred into 0.7 mm ID and 0.87 mm OD quartz capillary tubes from VitroCom, NJ, USA (sample height of 25 mm) and sealed on both ends with Cha-Seal^{TM} tube sealing compound (Medex International, Inc., USA). The samples were exposed to the white light from a halogen source (150 W halogen lamp) outside the ESR cavity at a stabilized temperature of $21 \pm 1\,^{\circ}C$. Two antioxidants, β-carotene and curcumin (both from Sigma-Aldrich), were used as singlet oxygen quenchers. ESR experiments were carried out using an ESP300E spectrometer (Bruker BioSpin GmbH), equipped with a standard rectangular mode TE_{102} cavity. Single-scan field-swept ESR spectra were recorded immediately after subsequent exposures of measured aliquots to illumination. The typical instrumental settings were: microwave frequency 9.38 GHz, microwave power 2.0 mW, sweep width 120 G, modulation frequency 100 kHz, modulation amplitude 0.5 G, receiver gain 4×10^4, time constant 20.48 ms, conversion time 40.96 ms and total scan time 41.9 s.

2.3. Near-infrared detection of $^1\Delta_g$ luminescence at 1270 nm

The potential of fullerol to photo-produce $^1\Delta_g$ was measured by direct detection of near-infrared steady state phosphorescence of singlet oxygen at 1270 nm. $^1\Delta_g$-phosphorescence

measurements were performed using a modified spectrofluorometer, SPEX Fluorolog-3, from Horiba Jobin-Yvon, which was equipped with a 450 W xenon lamp and a liquid nitrogen cooled InGaAs detector, model SPEX DSS-IGA020L. Spectra were recorded using 1 cm path length quartz cuvettes. The emission wavelength was selected using a long-pass filter ($\lambda > 850$ nm) and a 600 grooves mm^{-1} grid, which were installed in the emission monochromator of the spectrofluorometer. The photosensitization of singlet oxygen in the presence of $C_{60}(OH)_{19}(ONa)_{17}$ was brought on by illumination of the investigated solutions with 400 nm blue light selected by the excitation monochromator of Fluorolog-3. Rose Bengal (Sigma-Aldrich), a well-established photosensitizer of singlet oxygen, was used as a reference chromophore. The process of $^1\Delta_g$ formation in the presence of Rose Bengal was induced by illumination with 560 nm green light selected by the excitation monochromator of Fluorolog-3. Measurements of the characteristic 1270 nm phosphorescence were performed for formation of $^1\Delta_g$ in D_2O solutions supplemented with $C_{60}(OH)_{19}(ONa)_{17}$ or Rose Bengal. β-carotene from Sigma-Aldrich was used as a $^1\Delta_g$ inhibitor in this portion of the study.

2.4. Singlet oxygen-induced decomposition of tryptophan

The photosensitizing efficiency of $C_{60}(OH)_{19}(ONa)_{17}$ to generate singlet oxygen was checked in a photochemical decomposition assay, in which the decay of the tryptophan-related absorption band (220 nm) was monitored. The absorption spectra of aqueous solutions of tryptophan were acquired using a Varian Cary 50 UV–vis spectrophotometer. The studied solutions contained 20 μM concentrations of both tryptophan and $C_{60}(OH)_{19}(ONa)_{17}$. To generate $^1\Delta_g$, the samples were illuminated during short time intervals for a maximum total exposure time of 20 min. The water solutions of tryptophan supplemented with fullerol $C_{60}(OH)_{19}(ONa)_{17}$ were illuminated with monochromatic light ($\lambda = 400$ nm) from a custom-made blue LED-based source (30 mW). Haematoporphyrin, 8,13-bis(1-hydroxyethyl)-3,7,12,17-tetramethyl-21H,23H-porphine-2,18-dipropionic acid, herein referred to as HP, a well-established $^1\Delta_g$ generator, was used as a PS of reference in this study. HP was purchased from Sigma-Aldrich and used without any further purification. Prior to preparing water solutions, HP was dissolved in a small amount of ethanol. Then, the aliquots of HP stock solution in water were mixed with the aqueous solutions of tryptophan to achieve 1 μM concentration of HP and 50 μM concentration of tryptophan in the final solution. The UV–vis absorbance spectra were recorded using 1 cm path length quartz cuvettes. The photo-oxidative loss of tryptophan was monitored at the tryptophan-related absorption band (280 nm). Monochromatic light ($\lambda = 400$ nm) from the same light source as applied for exciting fullerol was used to excite the photosensitization process in the presence of HP.

2.5. Spin-labelled protein

Staphylococcal nuclease (SNase) is a small (16.8 kDa) single chain protein consisting of 149 amino acids. The protein was expressed in *E. coli* bacteria and then purified to apparent homogeneity by an automated liquid chromatography system. Prior to performing ESR measurements, SNase was spin-labelled. The general method for incorporating paramagnetic centres into proteins is called site-directed spin labelling (SDSL) and is based on selective cysteine mutagenesis [25]. In this study, we used an SNase mutant with the threonine-62 residue selectively targeted and mutated to cysteine (SNase T62C). The highly cysteine-reactive methanethiosulfonate spin label (MTSSL), 1-oxyl-2,2,5,5-tetramethyl-D3-pyrroline-3-methyl methanethiosulfonate, from Toronto Research Chemicals, North York, ON, was attached to the cysteine-62 residue (SNase T62C-SL). The ribbon representation of SNase and the location

Figure 2. The ribbon representation of SNase. The actual location of the MTSSL spin label at the amino acid residue 62 is marked by the grey arrow.

of the attachment of the MTSSL spin label in the SNase T62C mutant are shown in figure 2. MTSSL forms a covalent bond with the sulfide moiety on the cysteine residue. The unpaired spin (nitroxide group $NO^{\cdot}$) in MTSSL is incorporated into a five-membered ring, which contains one double bond. Therefore, the MTSSL spin probe is relatively rigid, compact and sensitive to the motion of the protein backbone. In many recent site-directed spin-labelling studies performed on proteins, MTSSL has been considered as a spin-label of choice [26].

The spin-labelled protein, T62C-SL, was then used as a molecular target for oxidative species generated in the presence of fullerol $C_{60}(OH)_{19}(ONa)_{17}$. Prior to the ESR measurements, T62C-SL spin-labelled protein was mixed with fullerol to obtain the final concentrations of 145 μM of SNase and 500 μM of fullerol. Subsequently, the solution was saturated with oxygen by bubbling O_2 for 30 min. Afterwards, aliquots of $\sim$7 μl of prepared solutions were transferred into 0.6 mm ID and 0.84 mm OD quartz capillaries and sealed at both ends in a similar way to that described above. The samples were then exposed to white light using the same experimental set-up as used for ESR scavenging of singlet oxygen (see section 2.2).

3. Results and discussion

3.1. ESR monitoring of singlet oxygen generation in aqueous solutions of fullerol $C_{60}(OH)_{19}(ONa)_{17}$

Photosensitization of $^1\Delta_g$ in the presence of fullerol $C_{60}(OH)_{19}(ONa)_{17}$ was quantified by measuring the growth of the characteristic ESR signal of TEMPOL, a paramagnetic product of singlet oxygen attack on the diamagnetic substrate, TMP–OH. The plots of the ESR signal intensity of TEMPOL as a function of illumination time in H_2O and D_2O solutions are shown in figure 3. The evolution of the ESR spectral features of TEMPOL in D_2O as a function of illumination time is shown in the inset to figure 3. In aqueous solutions, the ESR spectrum of TEMPOL consists of three narrow equidistant hyperfine lines with isotropic hyperfine constant $A_{iso} = 17.4$ G (inset to figure 3).

As could be expected for a singlet oxygen-mediated process, the observed reaction rate of TEMPOL production was about 10 times larger for D_2O solutions of $C_{60}(OH)_{19}(ONa)_{17}$. This result is consistent with the prolonged life-span of singlet oxygen in D_2O (up to about 60 μs in deuterium oxide, in contrast to about 3 μs in H_2O) [27]. Moreover, as shown in figure 4(b), the growth of the ESR signal of TEMPOL was entirely inhibited in solutions supplemented with a 100 μM concentration of singlet oxygen-scavenging antioxidants, β-carotene and curcumin. Both these antioxidants have been demonstrated to act as very efficient quenchers of singlet oxygen *in vitro* [28, 29].

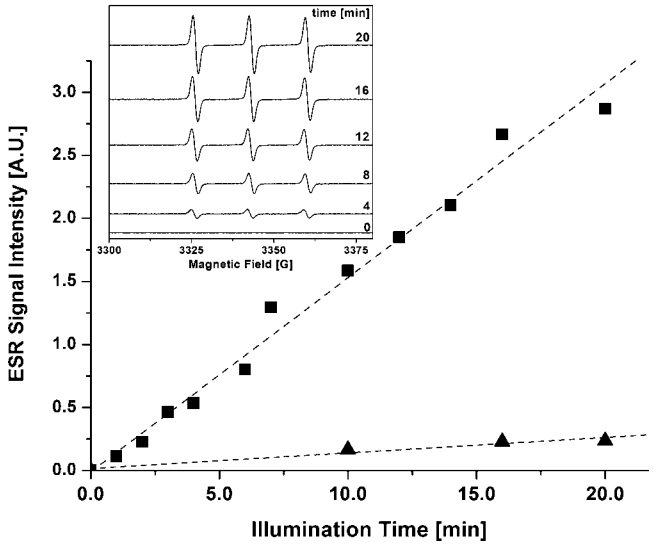

Figure 3. The growth of the ESR signal of TEMPOL as a function of illumination time observed for oxygenated H_2O (black triangles) and D_2O (black squares) solutions containing 2.5×10^{-4} M fullerol $C_{60}(OH)_{19}(ONa)_{17}$ and 2.5×10^{-2} M TMP–OH. Signal intensity was derived from the doubly integrated ESR traces of TEMPOL. Inset: evolution of the ESR signal of TEMPOL as a function of illumination time for singlet oxygen generation in oxygenated D_2O solution of $C_{60}(OH)_{19}(ONa)_{17}$.

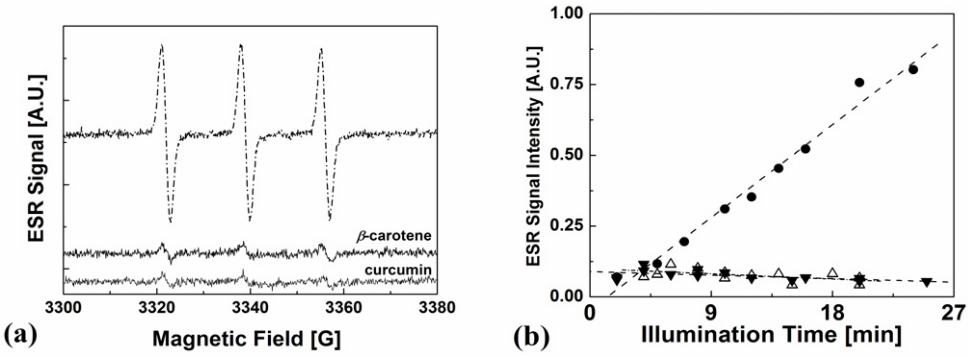

Figure 4. (a) ESR signal of TEMPOL after 20 min of illumination of D_2O solution containing fullerol $C_{60}(OH)_{19}(ONa)_{17}$ (6.9×10^{-4} M) and TMP–OH (5×10^{-2} M) in the absence of antioxidants (dash–dotted line) and in the presence of antioxidants, β-carotene (1×10^{-4} M) or curcumin (1×10^{-4} M). (b) Evolution of the ESR signal intensity derived from the doubly integrated ESR signal of TEMPOL as a function of illumination time for photosensitization of singlet oxygen in D_2O solutions of fullerol in the absence (filled circles) and presence of the antioxidants: β-carotene (empty triangles) and curcumin (filled triangles).

3.2. Fullerol-sensitized generation of singlet oxygen: measurements of near-infrared phosphorescence at 1270 *nm*

Experiments were done to monitor the highly specific O_2 ($^1\Delta_g$) $\rightarrow$ O_2 ($^3\Sigma_g^-$) singlet oxygen emission at 1270 nm. This near-infrared phosphorescence corresponding to $^1\Delta_g$-monomolecular decay is commonly considered as a 'fingerprint' of the formation of singlet

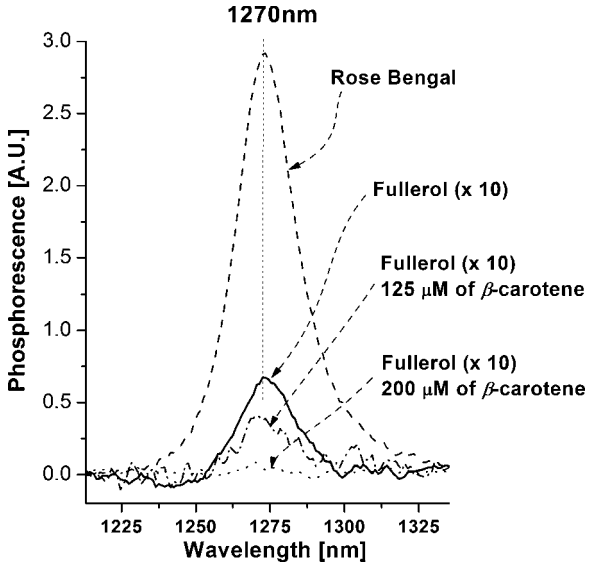

Figure 5. Near-infrared spectra at 1270 nm observed for photosensitization of singlet oxygen in D_2O in the presence of Rose Bengal (dotted trace) and fullerol $C_{60}(OH)_{19}(ONa)_{17}$ (solid trace). The marked inhibitory effect of β-carotene on the generation of $^1\Delta_g$ in the presence of fullerol $C_{60}(OH)_{19}(ONa)_{17}$ is also shown for two concentrations of the antioxidant: 125 μM (dashed–dotted trace) and 200 μM (dotted trace). The D_2O solutions containing PS were excited with the monochromatic light at 560 nm (Rose Bengal) and 400 nm (fullerol $C_{60}(OH)_{19}(ONa)_{17}$). Concentrations of PS were: 10 and 50 μM, for Rose Bengal and fullerol $C_{60}(OH)_{19}(ONa)_{17}$, respectively.

oxygen. Rose Bengal was used as the reference photosensitizer in these experiments. Rose Bengal is a synthetic dye from the xanthene family that exhibits strong absorption bands in the green area of the visible spectrum (480–580 nm). Rose Bengal is also known to produce singlet oxygen with high yields in aqueous milieus ($\Phi_\Delta = 0.76$ in D_2O) [30]. As can be seen in figure 5, the characteristic emission at 1270 nm was observed for both Rose Bengal and fullerol $C_{60}(OH)_{19}(ONa)_{17}$ in D_2O solutions. Clearly, the 1270 nm light emission detected for Rose Bengal was considerably stronger than for fullerol. Although relatively weak, the observed peak of phosphorescence at 1270 nm points to the generation of singlet oxygen in the presence of fullerol $C_{60}(OH)_{19}(ONa)_{17}$ via a type II photodynamic process. Thus, this spectroscopic finding provides direct evidence of the generation of singlet oxygen by the highly functionalized fullerene derivative used in this study. The quenching effect of β-carotene on the intensity of the 1270 nm phosphorescence spectrum was also observed. With increasing concentration of β-carotene, the 1270 nm emission intensity decreases and approaches values beyond the detection limit (figure 5).

The marked inhibitory effect of β-carotene (figure 5), which effectively neutralizes singlet oxygen by physical quenching (i.e. without chemical degradation) [31, 32], also points to a type II photoreaction mechanism for singlet oxygen formation in aqueous milieus containing fullerol $C_{60}(OH)_{19}(ONa)_{17}$.

3.3. Fullerol-mediated photo-oxidative damage to tryptophan: UV–vis absorbance study

Tryptophan, the largest amino acid residue of aromatic character, has long been known as a highly sensitive target for photo-oxidation through ROS, including singlet oxygen [33].

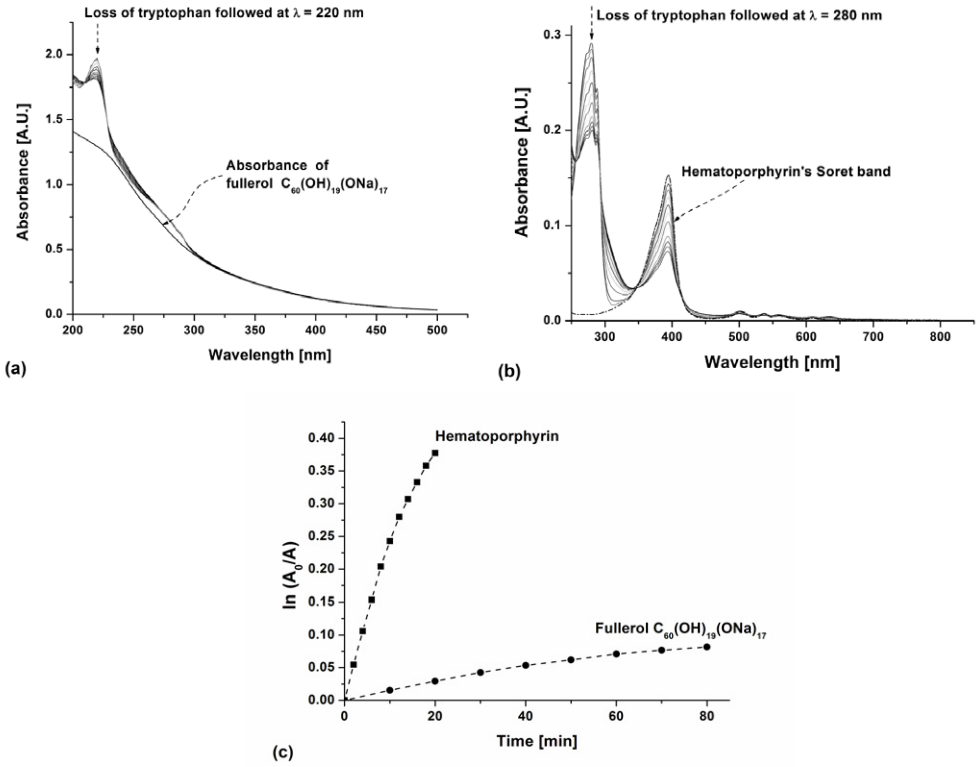

Figure 6. Photo-oxidative loss of tryptophan in the presence of fullerol $C_{60}(OH)_{19}(ONa)_{17}$ and haematoporphyrin. (a) UV–vis absorbance traces acquired for photo-oxidation of tryptophan in aqueous solution containing fullerol (20 μM) and tryptophan (20 μM). (b) Control measurement: UV–vis absorbance traces acquired for photo-oxidation of tryptophan in aqueous solution containing HP (1 μM) and tryptophan (50 μM). The UV–vis absorbance trace of HP before mixing with tryptophan is also shown (dashed–dotted trace). (c) Semilogarithmic plots $\ln(A_0/A)$ for the process of photodecomposition of tryptophan in the presence of fullerol (filled circles) and HP (filled squares). Both photosensitizers were excited with the monochromatic light $\lambda = 400$ nm (using the same blue LED light source). The total exposure time was 20 min for HP and 80 min for fullerol.

It is thought that tryptophan can quench singlet oxygen via physical and chemical routes. Interestingly, the rate constants for physical and chemical processes are of the same order of magnitude, i.e. $\sim$2–7 $\times$ 10^7 and 3 $\times$ 10^7 l mol^{-1} s^{-1}, respectively [34]. Tryptophan has two characteristic UV absorption bands centred at 220 and 280 nm, which can be used to monitor its loss under exposure to the oxidative stress [35]. In this study, we monitored the photo-oxidation of tryptophan to evaluate the efficiency of $C_{60}(OH)_{19}(ONa)_{17}$ for generation of singlet oxygen. This process was brought on by illumination with monochromatic light $\lambda = 400$ nm of the aqueous solution containing 20 μM of tryptophan and 50 μM of fullerol $C_{60}(OH)_{19}(ONa)_{17}$. The kinetics of photo-oxidation was monitored by following the decrease of the absorbance (A) at 220 nm for tryptophan. The corresponding absorbance traces showing the loss of tryptophan as a function of illumination time are shown in figure 6(a). A control experiment, performed for photo-oxidation of tryptophan in the presence of the reference photosensitizer, haematoporphyrin (HP), is shown in figure 6(b). The absorbance traces were acquired for the aqueous solution containing HP (1 μM) and tryptophan (50 μM), which was exposed to illumination with monochromatic light $\lambda = 400$ nm. In the presence of haematoporphyrin, the

kinetics of photodecomposition were monitored by following the decrease of the absorbance (A) at 280 nm for tryptophan. For both studied cases, the photodecomposition of tryptophan follows first-order kinetics with reference to tryptophan concentration. The corresponding first-order semilogarithmic plots $\ln(A_0/A)$ describing the progress of the photo-oxidation processes are shown in figure 6(c). In principle, the relative quantum yield of $^1\Delta_g$ generation by fullerol can be obtained by direct comparison of the slopes in the linear region of these plots. However, to precisely derive quantum efficiencies, a more quantitative experiment is needed to be performed with the same concentrations of fullerol and reference photosensitizer. This goal was, however, beyond the scope of this qualitatively oriented work.

In principle, the amino acid tryptophan used in this study as a substrate model for the compounds of biological interest can be photo-oxidized both by type I and type II reaction mechanisms [34]. Although our ESR scavenging and near-infrared emission experiments performed in the presence of fullerol suggested singlet oxygen formation, a free radical pathway in the photodecomposition of tryptophan cannot be discounted. Clearly, the absorbance spectra acquired during the photodecomposition of tryptophan in the presence of HP suggest a marked contribution of type I process. This can be seen from the photo-oxidative loss of the Soret band as the reaction progresses (figure 6(b)). This indicates that HP, in parallel to the type II mechanism that yields singlet oxygen, is also directly involved in the type I mechanism. This latter reaction pathway also leads to a partial photobleaching of the photosensitizer itself [30]. In contrast, as can be seen in figure 6(a), for the photosensitization process in the presence of fullerol there are no visible changes occurring to the photosensitizer's spectrum. This finding is in agreement with previous reports pointing to a high photostability of fullerene-based photosensitizers as compared with traditional organic photosensitizing compounds [36].

3.4. Fullerol-mediated photo-oxidative damage to the spin-labelled protein

In this study, we also report preliminary ESR results showing the impact of the photo-oxidative stress on the spin-labelled protein SNase. SNase is a toxin expressed by the bacterium *S. aureus*, which is a major human pathogen that has the capability of synthesizing a plethora of extracellular and cell-wall proteins, many of which are involved in various pathologies. SNase, a small (16.8 kDa) single chain protein consisting of 149 amino acids, has long been recognized as an excellent model for studies of protein folding and stability [37]. In this work, the spin-labelled protein, T62C-SL, was exposed to chemical, thermal and oxidative stress conditions. ESR was used to follow conformation changes of the spin-labelled protein exposed to the progressively intensified denaturing conditions. In particular, in this paper, we focus on the photo-oxidative stress-induced conformational changes occurring to T62C-SL in the presence of fullerol $C_{60}(OH)_{19}(ONa)_{17}$. The oxidative stress was brought on by illumination of the solution containing 145 μM of SNase and 500 μM of fullerol with polychromatic white light.

The ESR spectrum of SNase prior to illumination is shown in figure 7(a). Protein conformation changes were reported by the evolution of the molecular dynamics of MTSSL spin label. Since the MTSSL spin label located at residue 62 is relatively strongly immobilized within the protein structure, the corresponding ESR trace (figure 7(a)) exhibits two main spectral features: (i) a strong *slow* component consisting of the three broadened features, one central and two low- and high-field ESR lines which are denoted by $A_\parallel$ (parallel) and $A_\perp$ (perpendicular) hyperfine splitting, respectively, and (ii) a much weaker *fast* component consisting of two well-resolved narrow features, symmetrically spaced around the central feature (the central line of this set of ESR features overlaps with the strong central line of the *slow* component, denoted by A_{ISO} (ISO, isotropic hyperfine coupling) in figure 7(a). The

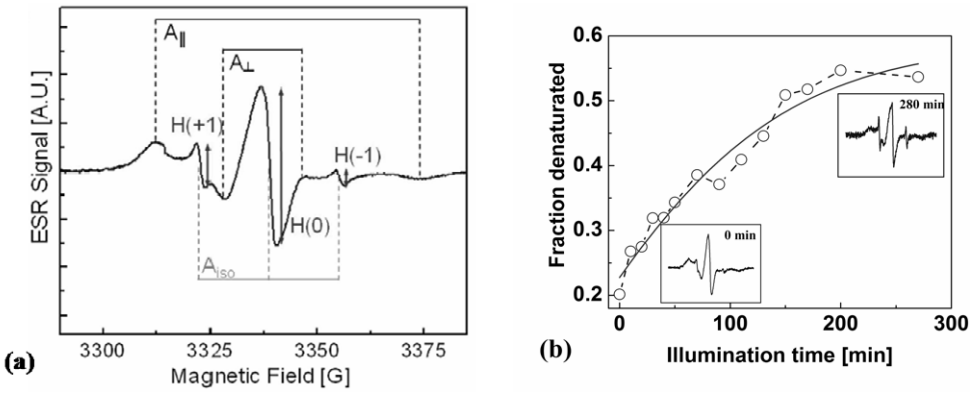

Figure 7. Fullerol-mediated photo-oxidative damage to the spin-labelled protein SNase T62C-SL. (a) The room temperature ESR spectrum of the spin-labelled SNase acquired prior to exposure to the oxidative stress. $A_{\perp}$, $A_{\parallel}$ and A_{ISO} represent the perpendicular, parallel and isotropic hyperfine splitting. (b) Oxidative stress-induced denaturation of the spin labelled SNase described by the fraction of denatured protein ($H_{(+1)}/H_{(0)}$) as a function of exposure to the oxidative stress. Insets: ESR spectra the T62C-SL SNase at two distinctive time points: prior to illumination and after 280 min of illumination in the presence of fullerol $C_{60}(OH)_{19}(ONa)_{17}$.

main broadened spectrum (i) accounts for the strongly immobilized spin labels and is therefore representative of the folded state of the T62C-SL. The low- and high-field extremes of this *slow*-motion spectrum correspond to the spin labels having their molecular planes oriented parallel to the external magnetic field. The *fast* component (ii) corresponds to the small fraction of faster tumbling nitroxide spins. The fast tumbling averages out the intrinsic g (Zeeman) and A (hyperfine) anisotropy of the nitroxide radical. This *fast* component of the ESR spectrum represents the fraction of unfolded proteins.

By all evidence, the T62C-SL SNase mutant exposed to the deleterious action of singlet oxygen was at least partially denatured (figure 7(b)). ESR spectra acquired as a function of exposure to the oxidative stress revealed a progressive increase of spectral features corresponding to less immobilized spin labels. This finding suggests an overall increase of the local dynamics of the protein backbone adjacent to the SL-anchoring sites. Thus, in this ESR experiment we could probe the denaturation process of the spin-labelled protein, T62C-SL SNase, which was exposed to the oxidative stress.

4. Conclusion

In this study, we have presented a comprehensive characterization of the photophysical properties of the novel, highly water-soluble derivative of C_{60}, fullerol $C_{60}(OH)_{19}(ONa)_{17}$. The measurements of the characteristic near infra-red phosphorescence of singlet oxygen at 1270 nm and ESR scavenging of the paramagnetic product of singlet oxygen attack confirmed that fullerol $C_{60}(OH)_{19}(ONa)_{17}$ is capable of photosensitizing the formation of singlet molecular oxygen ($^1\Delta_g$). To the best of our knowledge, the phosphorescence spectra of singlet oxygen at 1270 nm acquired in aqueous milieus containing a highly hydroxylated C_{60} derivative are the first of their kind.

Although singlet oxygen generation in the presence of fullerol $C_{60}(OH)_{19}(ONa)_{17}$ was substantially less efficient than in the presence of the well-known $^1\Delta_g$ producer, Rose Bengal, the potential of using fullerols in bio-oxidations is quite high. Strong assets of fullerols are

their low toxicity in the dark, high photostability (i.e. resistance to photobleaching), and their capability to photosensitize singlet oxygen within a particularly wide spectrum of illumination, ranging from UV to visible light. Therefore, fullerols might be used as photosensitizers in general sterilization or for selective treatment of bacterial infections via photodynamic inactivation [38].

We have also shown that a combination of ESR and SDSL, which is a well-established tool for studying structural transitions accompanying protein denaturation or folding, can also be used for monitoring changes in protein conformation induced by oxidative stress. These alterations in protein conformation were observed for a spin-labelled protein (SNase T62C-SL) in an aqueous solution containing the photosensitizer fullerol $C_{60}(OH)_{19}(ONa)_{17}$. We associate these changes with photo-generation of singlet oxygen in the presence the water-soluble C_{60} derivative via the type II reaction mechanism, which is then followed by singlet oxygen attack on amino acid residues of the protein. Although our spectroscopic studies based on the photo-oxidative loss of tryptophan, characteristic phosphorescence of singlet oxygen at 1270 nm, and, finally, ESR scavenging, point to $^1\Delta_g$ as the major initiator of the photo-oxidative damage, it is important to note that the role of other ROS cannot be discounted. Further studies elucidating other ROS (by appropriate spin-trapping) in combination with methods characterizing the oxidized products are necessary to fully unveil photo-oxidative processes involving biomolecules in the presence of water-soluble derivatives of C_{60}. Nonetheless, here we have shown that the photobiological risk associated with the use of a water-soluble derivative of C_{60} might be due to the formation of singlet molecular oxygen via a type II photoreaction mechanism. This is of particular importance for fullerols, given their wide-spread applications in products designed for direct human use and consumption.

Acknowledgments

We thank Professor W E Stites, Department of Chemistry and Biochemistry, University of Arkansas, Fayetteville, for providing us with the SNase clones. We are also very grateful to Micara Larion, Department of Chemistry and Biochemistry, Florida State University (FSU), Tallahassee, for purification of the protein used in this study. AS and BV acknowledge the support of the Centre of Excellence for Advanced Spectroscopy Applications in Physics, Modern Science, Biology and Environmental Protection–ASPECT (the European Community contract GMA1-2002-72801). The research portion at the EPFL in Lausanne was partially supported by the Swiss National Science Foundation and the Nano2Life European Network.

References

[1] Finkel T and Holbrook N J 2000 *Nature* **408** 239–47
[2] Mattson M P 2004 *Nature* **430** 631–9
[3] Beckman K B and Ames B N 1998 *Physiol. Rev.* **78** 547–81
[4] Kamat J P and Devasagayam T P A 2000 *Toxicology* **155** 73–82
[5] Davies M J 2005 *Biochim. Biophys. Acta* **1703** 93–109
[6] Tabner B J, Turnbull S, El-Agnaf O and Allsop D 2001 *Curr. Top. Med. Chem.* **1** 507–17
[7] Briviba K, Klotz L O and Sies H 1997 *Biol. Chem.* **378** 1259–65
[8] Baier J, Maisch T, Maier M, Engel E, Landhaler M and Baumler W 2006 *Biophys. J.* **91** 1452–9
[9] Davies M J 2004 *Photochem. Photobiol. Sci.* **3** 17–25
[10] Biasutti M A, Soltermann A T and Garcia N A 2000 *J. Peptide Res.* **55** 41–50
[11] Liao J C, Roider J and Jay D J 1994 *Proc. Natl Acad. Sci. USA* **91** 2659–63
[12] Calin M A, Gruia M, Herascu N and Coman T 2004 *J. Exp. Theor. Oncol.* **4** 247–51
[13] Bosi S, Da Ros T, Spalluto G and Prato M 2003 *Eur. J. Med. Chem.* **38** 913–23
[14] Dugan L L, Gabrielsen J K, Yu S P, Lin T S and Choi D W 1996 *Neurobiol. Dis.* **3** 129–35

[15] Xia T, Kovochich M, Brant J, Hotze M, Sempf J, Oberley T, Sioutas C, Yeh J I, Wiesner M R and Nel A E 2006 *Nano Lett.* **6** 1794–807
[16] Vileno B, Lekka M, Sienkiewicz A, Marcoux P R, Kulik A J, Kasas S, Catsicas S, Graczyk A and Forró L 2005 *J. Phys.: Condens. Matter* **17** S1471–82
[17] Vileno B, Marcoux P R, Lekka M, Sienkiewicz A, Fehér T and Forró L 2006 *Adv. Funct. Mater.* **16** 120–8
[18] Guldi D and Prato M 2000 *Acc. Chem. Res.* **33** 695–703
[19] Prat F, Stackow R, Bernstein R, Qian W, Rubin Y and Foote C S 1999 *J. Phys. Chem.* A **103** 7230–5
[20] Sayes C, Fortner J, Lyon D, Boyd A, Ausman K, Guoh W, Tao Y, Sitharaman B, Wilson L, West J and Colvin V 2004 *Nano Lett.* **4** 1881–7
[21] Isakovic A, Markovic Z, Todorovic-Markovic B, Nikolic N, Vranjes-Djuric S, Mirkovic M, Dramicanin M, Harhaji L, Raicevic N, Nikolic Z and Trajkovic V 2006 *Toxicol. Sci.* **91** 173–83
[22] Chiang L Y, Upasani R B and Swirczewski J W 1992 *J. Am. Chem. Soc.* **114** 10154–7
[23] Lion Y, Delmelle M and Van de Vorst A 1976 *Nature* **263** 442–3
[24] Ando T, Yoshikawa T, Tanigawa T, Kohno M, Yoshida N and Kondo M 1997 *Life Sci.* **61** 1953–9
[25] Hubbell W L, Gross A, Langen R and Lietzow M A 1998 *Curr. Opin. Struct. Biol.* **8** 649–56
[26] Columbus L and Hubbell W L 2002 *Trends Biochem. Sci.* **27** 288–95
[27] Andersen L K and Ogilby P R 2002 *J. Phys. Chem.* A **106** 11064–9
[28] Di Mascio P, Kaiser S and Sies H 1989 *Arch. Biochem. Biophys.* **274** 532–8
[29] Maheshwari R K, Singh A K, Gaddipati J and Srimal R C 2006 *Life Sci.* **78** 2081–7
[30] DeRosa M C and Cruchtley R J 2002 *Coord. Chem. Rev.* **233/234** 351–71
[31] Stahl W and Sies H 1996 *Arch. Biochem. Biophys.* **336** 1–9
[32] Sies H and Stahl W 2004 *Photochem. Photobiol. Sci.* **3** 749–52
[33] Creed D 1984 *Photochem. Photobiol.* **39** 537–62
[34] Matheson I B C, Etheridge R D, Kratowitch N R and Lee J 1975 *Photochem. Photobiol.* **21** 165–71
[35] Rasheed Z, Khan M W A and Ali R 2006 *Autoimmunity* **39** 479–88
[36] Arbogast J W and Foote C S 1991 *J. Am. Chem. Soc.* **113** 8886–9
[37] Shortle D 1995 *Adv. Prot. Chem.* **46** 217–47
[38] Caminos D A, Spesia M B and Durantini E N 2006 *Photochem. Photobiol. Sci.* **5** 56–65